Diagn Interv Radiol 2024; DOI: 10.4274/dir.2024.242652

PEDIATRIC RADIOLOGY

ORIGINAL ARTICLE

Cortical and subcortical structural changes in pediatric patients with infratentorial tumors

Barış Genç[1]
Kerim Aslan[1]
Derya Bako[1]
Semra Delibalta[2]
Meltem Necibe Ceyhan Bilgici[1]

[1]Ondokuz Mayıs University Faculty of Medicine, Department of Neuroradiology, Samsun, Türkiye

[2]Acıbadem University, Atakent Hospital, Clinic of Radiology, İstanbul, Türkiye

PURPOSE

This study aimed to detect supratentorial cortical and subcortical morphological changes in pediatric patients with infratentorial tumors.

METHODS

The study included 24 patients aged 4–18 years who were diagnosed with primary infratentorial tumors and 41 age- and gender-matched healthy controls. Synthetic magnetization-prepared rapid gradient echo images of brain magnetic resonance imaging were generated using deep learning algorithms applied to T2-axial images. The cortical thickness, surface area, volume, and local gyrification index (LGI), as well as subcortical gray matter volumes, were automatically calculated. Surface-based morphometry parameters for the patient and control groups were compared using the general linear model, and volumes between subcortical structures were compared using the t-test and Mann–Whitney U test.

RESULTS

In the patient group, cortical thinning was observed in the left supramarginal, and cortical thickening was observed in the left caudal middle frontal (CMF), left fusiform, left lateral orbitofrontal, left lingual gyrus, right CMF, right posterior cingulate, and right superior frontal ($P < 0.050$). The patient group showed a volume reduction in the pars triangularis, paracentral, precentral, and supramarginal gyri of the left hemisphere ($P < 0.05$). A decreased surface area was observed in the bilateral superior frontal and cingulate gyri ($P < 0.05$). The patient group exhibited a decreased LGI in the right precentral and superior temporal gyri, left supramarginal, and posterior cingulate gyri and showed an increased volume in the bilateral caudate nucleus and hippocampus, while a volume reduction was observed in the bilateral putamen, pallidum, and amygdala ($P < 0.05$). The ventricular volume and tumor volume showed a positive correlation with the cortical thickness in the bilateral CMF while demonstrating a negative correlation with areas exhibiting a decreased LGI ($P < 0.05$).

CONCLUSION

Posterior fossa tumors lead to widespread morphological changes in cortical structures, with the most prominent pattern being hypogyria.

CLINICAL SIGNIFICANCE

This study illuminates the neurological impacts of infratentorial tumors in children, providing a foundation for future therapeutic strategies aimed at mitigating these adverse cortical and subcortical changes and improving patient outcomes.

KEYWORDS

Medulloblastoma, neoplasms, brain, primary, hippocampus, amygdala

Corresponding author: Barış Genç

E-mail: barisgenc12@gmail.com

Received 09 January 2024; revision requested 06 February 2024; last revision received 15 April 2024; accepted 15 May 2024.

Epub: 03.06.2024

Publication date: 09.09.2024

DOI: 10.4274/dir.2024.242652

Central nervous system neoplasms are the most common solid tumors in children. With advancing therapies, the 10-year survival rate in these patients is approximately 70%. Posterior fossa tumors are more frequently observed in childhood, and the most common pediatric posterior fossa tumors are medulloblastomas and astrocytomas.[1] Although

You may cite this article as: Genç B, Aslan K, Bako D, Delibalta S, Ceyhan Bilgici MN. Cortical and subcortical structural changes in pediatric patients with infratentorial tumors. *Diagn Interv Radiol*. 2024;30(5):328-334.

astrocytomas can achieve a cure with total resection, medulloblastomas require chemotherapy and radiotherapy treatments after resection.[2]

Neuroplasticity is the brain's ability to change functionally, connectively, or structurally in physiological or pathological conditions. Recent advancements in neuroimaging have demonstrated that the brain can reorganize itself after pathologies, such as traumatic brain injury, stroke, and tumors, particularly in adults.[3] Children are more successful than adults in learning complex skills, such as learning a new language or playing a new instrument.[4,5] Children with unilateral left-brain damage at an early age can develop normal language skills, while lesions of similar location and extent in the adult brain cause more aphasia.[6]

Recent studies have been conducted on changes occurring in the contralateral hemisphere secondary to supratentorial gliomas in adults, but these studies are generally voxel-based morphometry (VBM) studies investigating changes in gray matter volume.[7] Surface-based morphometry (SBM) provides parameters such as cortical thickness, sulcal folding, and surface area that cannot be obtained with VBM. Furthermore, SBM is more successful than VBM at the intersections of gray and white matter.[8] In their SBM study, Zhang et al.[9] detected widespread changes in the contralateral hemisphere in adult patients with frontal low-grade glioma (LGG) for the first time using virtual brain grafting, and these changes were not detected in a VBM study conducted in a similar group.[7]

The posterior fossa contains the cerebellum and the brainstem. The dentate nucleus in the cerebellum is highly advanced in monkeys and humans, with dentothalamic and thalamocortical pathways projecting to the prefrontal cortex.[10,11] Recent studies show that the cerebellum is no longer merely an organ associated with balance but actively participates in cognitive events, speech, and complex motor functions.[10] Cerebellar cognitive affective syndrome is a condition of cognitive decline in patients with cerebellar lesions, and its physiopathology is not fully understood.[12] A VBM study conducted on children who were cured after a posterior fossa tumor detected reduced gray matter volume in the entorhinal cortex, thalamus, hypothalamus, corpus callosum, and cuneus.[13] However, this could be due to the disease itself or secondary to chemoradiotherapy.[14]

There are no studies investigating cortical and subcortical changes at the time of diagnosis in children with posterior fossa tumors. There are several reasons for this. First, although they are the most common solid tumors in childhood, they are relatively rare.[1] Myelination is rapid in the first 2 years of life, and medulloblastomas peak at the age of 3 years.[15] Surface construction algorithms, such as Freesurfer, require good image contrast and can be applied to anatomically normal or near-normal brains without significant morphological abnormalities. In the presence of an intracranial tumor, Freesurfer has a failure rate of up to 30% in cortical reconstruction.[16] Therefore, it has prevented the detection of cortical and subcortical changes in pediatric tumors. Although virtual brain grafting studies have made this possible, they require neuroanatomical experience and time.[17] Recently, however, software developed using deep learning has made surface reconstruction possible in tumoral diseases by producing synthetic magnetization-prepared rapid gradient echo (MP-RAGE) images.[18]

Our aim in this study is to investigate supratentorial cortical and subcortical morphological changes in pediatric posterior fossa tumors.

Main points

- Pediatric posterior fossa tumors cause widespread hypogyrification and reductions in surface and volume, while also leading to an increase in cortical thickness.
- Pediatric posterior fossa tumors lead to an increase in volume in the hippocampus and caudate nucleus, while also causing an increase in the volume of the putamen, pallidum, and amygdala.
- Cortical and subcortical morphological changes have shown a correlation with ventricular volume and tumor volume.

Methods

This study was designed retrospectively. Ondokuz Mayıs University Clinical Research and Ethics Committee (decision no: 2023/300, date: 10.10.2023) approval has been obtained. All participants were fully informed and gave their written informed consent prior to each examination. Guidelines from Strengthening the Reporting of Observational Studies in Epidemiology were carefully followed.[19]

Participants

Patients aged <18 years who underwent brain magnetic resonance imaging (MRI) due to intracranial tumor in the unit between 2015 and 2023 were retrospectively screened. Among these patients, those with a posterior fossa tumor who did not receive any treatment (chemoradiotherapy, surgery, steroids) before the MRI and who were diagnosed pathologically after the MRI were included in the study. Children aged <4 years were excluded from the study due to insufficient myelination. Children who did not have any chronic diseases, who presented with non-specific symptoms, whose brain MRI did not reveal any pathology, and who were age- and gender-matched formed the control group (Figure 1).

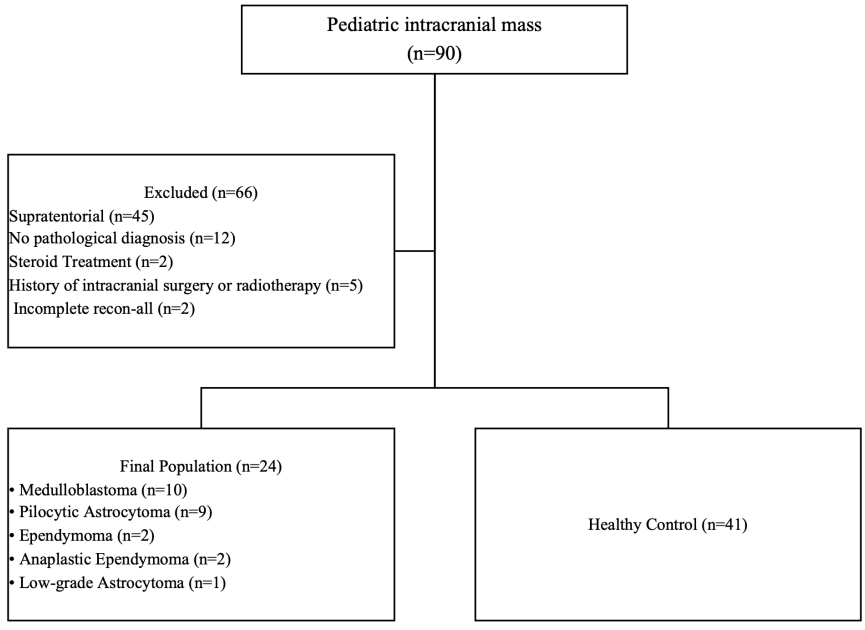

Figure 1. Flowchart of study.

Magnetic resonance imaging acquisition

MRI was performed on the patient and control groups with one of two devices with a magnetic field strength of 1.5 Tesla (Philips, Achieva, Best, the Netherlands) or 3 Tesla (Philips, Ingenia, Best, the Netherlands).

The MRI protocol for patients who had a 3 Tesla scan was as follows: T2W-axial turbo spin-echo sequence [repetition time (TR)/ echo time (TE), 3,000/80 ms; section thickness, 5 mm; matrix, 261 × 384; number of excitations (NEX), 3], 3D fluid attenuation inversion recovery (FLAIR) coronal (TR/TE/TI, 4,800/381/1,650 ms; section thickness, 3 mm; NEX, 2). For patients who had a 1.5 Tesla scan, the protocol was as follows: T2W-axial turbo spin-echo sequence (TR/TE, 8,078/100 ms; section thickness, 4 mm; matrix, 242 × 250; NEX, 4), T2-FLAIR coronal (TR/TE/TI, 7,000/140/2,800 ms; section thickness, 4 mm; NEX, 2).

Magnetic resonance imaging processing

Due to the different devices and a heterogeneous data set, SynthSR 2.0 was used in the Freesurfer developer version. SynthSR is a deep learning-based tool that enables the creation of synthetic MP-RAGE images for surface-based analyses with high accuracy, even if the images obtained clinically are heterogeneous. Moreover, it is challenging to perform surface-based analysis with Freesurfer in patients with intracranial tumors. SynthSR overcomes this challenge.

The synthetic MP-RAGE images were generated from T2-axial images with SynthSR.[18] Then, pre-processing for cortical thickness, surface area, volume, and local gyrification index (LGI) analyses and cortical reconstruction were performed using the standard Freesurfer (V 7.4.0). To increase the accuracy of surface reconstruction, synthetic MP-RAGE images were used together with T2-FLAIR images (Figure 2).

Tumor masking

A proficient general radiologist judiciously utilized the volume of interest procedure within the ITK-SNAP software suite to construct masks representing tumor volumes.

Statistical analysis

Demographic information of the patient and control groups, the magnetic field strength, estimated total intracranial volume (eTIV), and normalized subcortical volume (structure volume × 1.000/eTIV); data were compared using the chi-squared test, t-test, or Mann–Whitney U test.

Maps of cortical thickness, volume, and surface area for each patient were registered to the "fsaverage" template included in Freesurfer, and a generalized linear model (GLM) was then generated. Age, gender, and magnetic field strength were used as covariates for the GLM. Smoothing was applied to the cortical thickness, to volume maps with a full width at half maximum (FWHM) of 10 mm, to surface area maps with an FWHM of 15 mm, and to LGI maps with an FWHM of 25 mm. The patient and control groups were compared using "mri_glmfit" and the main results were analyzed using "mri_glmfit-sim," with 1.000 random permutations. To prevent false positive results, the cluster-wise *P* threshold was set at 0.05, and the vertex-wise cluster threshold was set at 10^{-3}.[20]

When a significant group difference was detected, the mean cortical thickness, surface area, volume, and LGI parameters in the significant cluster for each participant were extracted using the "mri_segstats" command. Volumes of subcortical structures were calculated using "asegstats2table." The Spearman correlation coefficient (rho) was calculated to evaluate the correlation between these parameters and the total volume of the lateral ventricles and the volume of the tumor. A *P* value of <0.05 was considered statistically significant.

Results

Clinical and demographic characteristics: the final population of the study consisted of 24 patients with posterior fossa tumors and 41 age- and gender-matched healthy controls. The patient group was aged 8.2 ± 4.2 years, and the control group was aged 10.9 ± 3.7 years; there was no statistically significant difference in ages between the groups ($P = 0.11$). No significant difference was detected in the magnetic field strength between the patient and control groups in the chi-squared test ($P = 0.08$). In the patient group, 10 received pathological diagnoses of medulloblastoma, 9 of pilocytic astrocytoma, 2 of ependymoma, 2 of anaplastic ependymoma, and 1 of low-grade astrocytoma. All lesions were located in the posterior fossa. The median size of the tumors was 22.1 mL (interquartile range: 22.3 mL). Seventeen of the lesions caused hydrocephalus, and the average lateral ventricular volume for the patient group was 39.9 ± 26.0 cm^3.

Cortical morphological changes

Cortical thickness: The patient group demonstrated a reduction in cortical thickness in the left supramarginal gyrus ($P = 0.010$, size: 221 mm^2) and left superior frontal gyrus ($P = 0.018$, size: 200 mm^2); an increase in cortical thickness was observed in the left caudal middle frontal (CMF) gyrus ($P = 0.0002$, size: 1,249 mm^2), left fusiform gyrus ($P = 0.001$, size: 327 mm^2), left lateral orbitofrontal gyrus ($P = 0.04$, size: 168 mm^2), left lingual gyrus ($P = 0.033$, size: 179 mm^2), right CMF gyrus ($P = 0.0002$, size: 727 mm^2), right posterior cingulate gyrus ($P = 0.0002$, size: 363 mm^2), right superior frontal gyrus ($P = 0.004$, size: 256 mm^2), and right lateral orbitofrontal gyrus ($P = 0.049$, size: 162 mm^2) (Figure 3, Table 1).

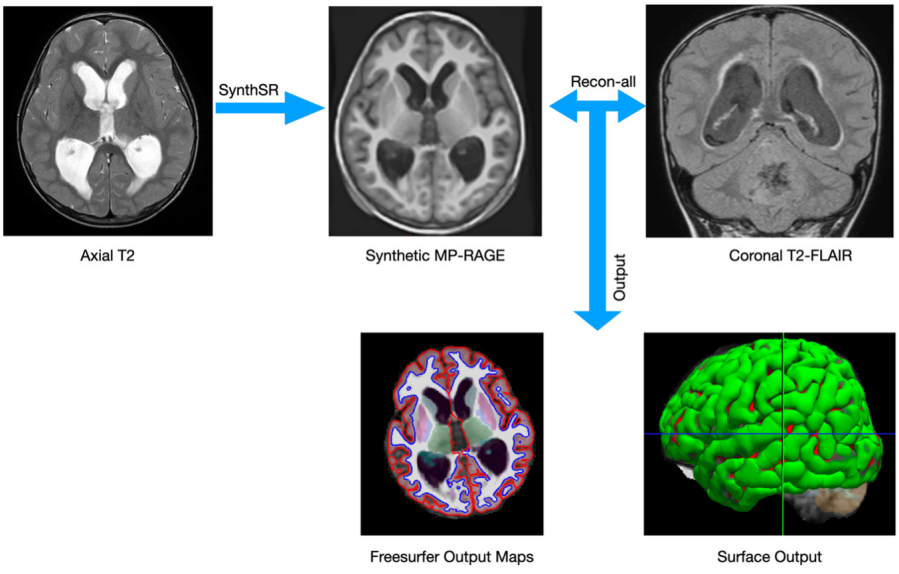

Figure 2. The cortical reconstruction pipeline. MP-RAGE, magnetization-prepared rapid gradient echo; FLAIR, fluid attenuation inversion recovery.

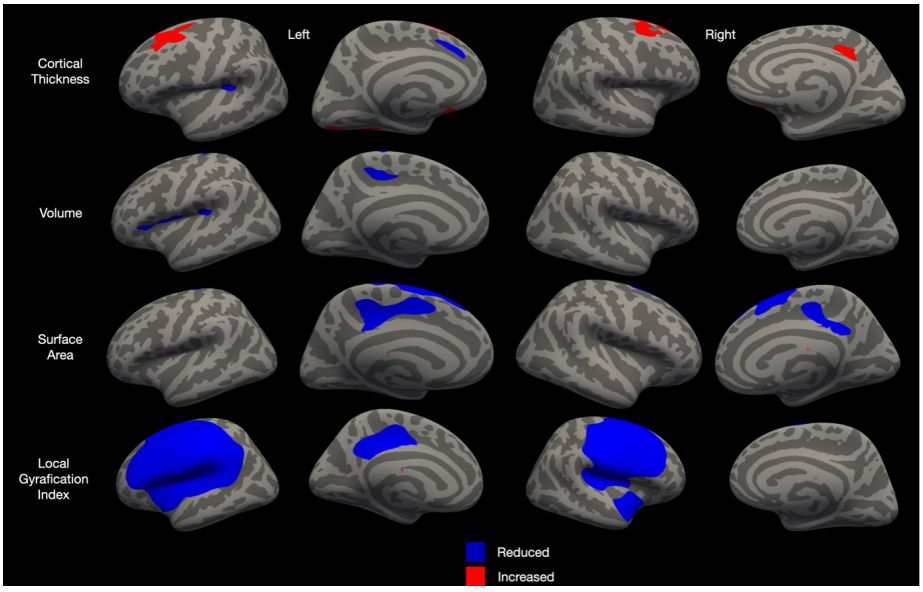

Figure 3. Areas showing changes in cortical thickness, surface area, volume, and local gyrification index in cases with posterior fossa tumors.

Table 1. The comparison of cortical morphology at the vertex level reveals significant clusters

Measurement	Group comparison	Cluster	Peak MNI coordinates	Size (mm^2)	*P* value of CWP
Cortical thickness	HC > patient	L. supramarginal	−34, −35, 17	221	0.010
		L. superior frontal	−10, 31, 31	200	0.018
		L. caudal middle frontal	−34, 13, 50	1,249	<0.001
	Patient > HC	L. fusiform	−28, −48, −18	327	0.001
		L. lingual	−19, −85, −10	179	0.033
		L. lateral orbitofrontal	−14, 12, −15	168	0.049
		R. caudal middle frontal	32, 13, 50	727	<0.001
		R. posterior cingulate	12, −36, 50	363	<0.001
		R. superior frontal	14, 38, 46	256	0.004
		R. lateral orbitofrontal	17, 23, −22	162	0.049
Volume	HC > patient	L. pars triangularis	−33, 27, 8	385	0.001
		L. paracentral	17, −26, 42	248	0.009
		L. precentral	−10, −25, 74	238	0.012
		L. supramarginal	−35, −33, 20	217	0.023
Local gyrification index	HC > patient	L. supramarginal	−52, −31, 35	23,075	<0.001
		L. posterior cingulate	−9, −26, 39	1,647	<0.001
		R. precentral	52, −5, 43	14,342	<0.001
		R. superior temporal	48, 6, −20	1,357	<0.001

All clusters survived correction for multiple comparisons using a Monte Carlo simulation, resulting in a corrected cluster-wise $P < 0.05$. L, left; R, right; HC, healthy control; MNI, The Montreal Neurological Institute; CWP, cluster-wise probability.

Volume: The patient group showed a decrease in volume in the left pars triangularis ($P = 0.001$, size: 385 mm^2), left paracentral gyrus ($P = 0.009$, size: 248 mm^2), left precentral ($P = 0.012$, size: 238 mm^2), and left supramarginal gyrus ($P = 0.023$, size: 217 mm^2). No statistically significant volume change was observed in the right hemisphere (Figure 3, Table 1).

Surface area: The patient group showed a decrease in surface area in the left posterior cingulate ($P = 0.0004$, size: 986 mm^2), left superior frontal ($P = 0.001$, size: 554 mm^2), right superior frontal ($P = 0.0002$, size: 1,737 mm^2), and right isthmus cingulate ($P = 0.003$, size: 774 mm^2). No area increase in the patient group was observed (Figure 3, Table 1).

Local gyrification index: In the patient group, a decrease in the LGI was observed in the right hemisphere's precentral gyrus ($P = 0.0002$, size: 14,342 mm^2), right superior temporal gyrus ($P = 0.0002$, size: 1,357 mm^2), left hemisphere's supramarginal gyrus ($P = 0.0002$, size: 23,075 mm^2), and posterior cingulate gyrus ($P = 0.0002$, size: 1,647 mm^2) (Figure 3, Table 1).

Correlation

The ventricular volume showed a positive correlation with cortical thickness in the areas of bilateral CMF gyrus where a cortical thickness increase was observed [right: ($P < 0.0001$, rho: 0.74); left: ($P = 0.0049$, rho: 0.57)]. The cortical thickness of the cluster in the right CMF gyrus showed a positive correlation with tumor volume ($P = 0.015$, rho: 0.50) but did not correlate with the left cluster.

The LGI showed a negative correlation with the ventricular volume in the cluster containing the right precentral gyrus ($P = 0.0001$, rho: −0.72), right superior temporal gyrus ($P = 0.0011$, rho: −0.64), left supramarginal gyrus ($P < 0.0001$, rho: −0.77), and the left posterior cingulate gyrus ($P = 0.0003$, rho: −0.70). The LGI showed a negative correlation with the tumor volume in the cluster containing the right precentral gyrus ($P = 0.015$, rho: −0.50), left supramarginal gyrus ($P = 0.033$, rho: −0.44), and the peak cluster in the left posterior cingulate gyrus ($P = 0.0021$, rho: −0.61).

No significant correlation was observed between the tumor volume and ventricular volume in areas where the cortical volume changed ($P > 0.05$).

Subcortical volumetric findings

When compared with the control group, the posterior fossa tumor group showed volume increases in the left caudate ($d = 1.37$, $P < 0.0001$), right caudate ($d = 1.50$, $P < 0.0001$), left hippocampus ($d = 0.99$, $P = 0.0006$), and right hippocampus ($d = 1.02$, $P = 0.0049$), and volume decreases in the left putamen ($d = -1.16$, $P < 0.0001$), right putamen ($d = -1.45$, $P < 0.0001$), left pallidum ($d = 0.99$, $P = 0.0006$), right pallidum ($d = 0.77$, $P = 0.0131$), left amygdala ($d = -0.47$, $P = 0.024$), and right amygdala ($d = 1.11$, $P = 0.0003$). No statistically significant volume difference was observed in the bilateral thalamus between the groups (Table 2).

Correlation of subcortical structures

The tumor volume showed a negative correlation with the volume of the left amygdala ($P = 0.02$, rho: −0.48) and the left accumbens area ($P = 0.047$, rho: −0.41) but showed a positive correlation with the volume of the bilateral caudate nucleus [right: ($P = 0.001$, rho: 0.62); left: ($P = 0.027$, rho: 0.46)]. No statistically significant correlation was observed with other subcortical structures (Figure 4, Table 3).

The total ventricular volume showed a negative correlation with the bilateral putamen [right: ($P = 0.003$, rho: −0.59); left: ($P = 0.023$, rho: −0.46)], bilateral pallidum [right: ($P = 0.006$, rho: −0.54); left: ($P = 0.0002$, rho: −0.71)], bilateral accumbens area [right: ($P = 0.017$, rho: −0.48); left: ($P = 0.0001$, rho: −0.72)], and a positive correlation with the bilateral caudate nucleus [right: ($P = 0.011$, rho: 0.51); left: ($P = 0.02$, rho: −0.47)], and left hippocampus ($P = 0.012$, rho: 0.51) (Figure 4, Table 3).

Discussion

In this study, we investigated the cortical morphological and subcortical volumetric changes at the time of diagnosis and their relationship with tumor size and ventricular volume in children with posterior fossa tumors. Our findings demonstrated a cortical thickening, particularly in the bilateral CMF region, even at the time of diagnosis. We observed volume reduction in the left supramarginal gyrus, surface area reduction in the posterior cingulate and superior frontal gyrus, and widespread hypogyrification in the bilateral fronto-temporo-parietal areas. Whereas the volume of the caudate nucleus and hippocampus increased, the putamen, amygdala, and nucleus accumbens showed volume reduction. These cortical and subcortical changes exhibited a significant association with ventricular volume, whereas only a partial relationship was observed with tumor size.

To our knowledge, the question of whether there are structural changes in the brain in childhood tumors has not been investigated. Large-scale studies are challenging due to the relative rarity of these tumors. Additionally, for such research, appropriate analysis of children's brain images and standardization of MRI devices are necessary. The SynthSR 2.0 used in our study enables the creation of suitable images for surface-based analysis and allows surface-based analysis even in the presence of intracranial tumors, making it feasible to work with heterogeneous datasets.[18]

Clinical and neuroimaging studies have shown that the cerebellum is not only involved in motor control or balance but also plays a role in a range of cognitive functions, such as language, emotion processing, and attention.[10] The cerebellum contains circuits associated with various areas, including the prefrontal cortex, parietal cortex, thalamus, superior temporal region, and limbic system.[21] Cerebellar cognitive affective syndrome is an entity described in the last 25

Table 2. The comparison of subcortical gray matter volume of patient and healthy control group

Structure volume (mL)	HC (n = 41)	Patient (n = 24)	Cohen's D	*P*
Left thalamus	4.71 ± 0.37	4.75 ± 0.41	−0.10	0.697
Left caudate	2.29 ± 0.25	2.76 ± 0.46	1.37	<0.001*
Left putamen	3.42 ± 0.28	3.05 ± 0.38	−1.16	0.001*
Left pallidum	1.13 ± 0.1	1.06 ± 0.15	−0.51	0.084
Left hippocampus	2.87 ± 0.2	3.31 ± 0.68	0.99	<0.001*
Left amygdala	1.01 ± 0.1	0.94 ± 0.22	−0.47	0.025*
Left accumbens area	0.47 ± 0.06	0.37 ± 0.06	−1.67	<0.001
Right thalamus	4.51 ± 0.32	4.48 ± 0.34	−0.09	0.736
Right caudate	2.36 ± 0.28	2.86 ± 0.42	1.50	<0.001*
Right putamen	3.38 ± 0.26	2.95 ± 0.34	−1.45	<0.001
Right pallidum	1.21 ± 0.13	1.08 ± 0.22	−0.77	0.013
Right hippocampus	2.89 ± 0.25	3.33 ± 0.62	1.02	0.005*
Right amygdala	1.16 ± 0.11	1.03 ± 0.15	−1.11	<0.001
Right accumbens area	0.44 ± 0.07	0.38 ± 0.06	−0.91	<0.001
Total lateral ventricle	8.18 ± 3	39.94 ± 26.04	2.00	<0.001*

*The Mann–Whitney U test performed. HC, healthy control.

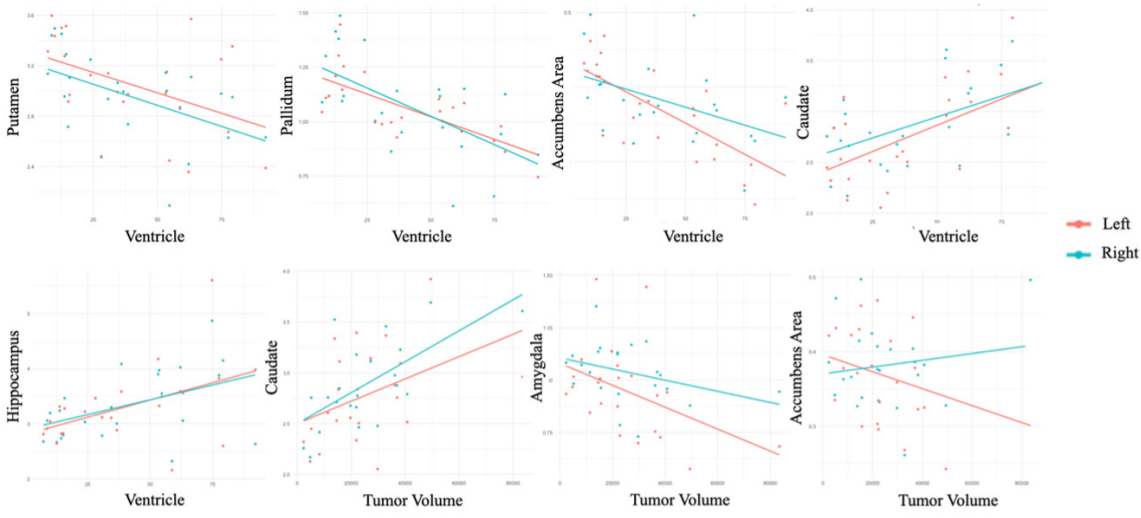

Figure 4. Scatterplot demonstrating the correlation between subcortical gray matter volumes and tumor volume, as well as the correlation between subcortical gray matter volumes and ventricular volume.

Table 3. The correlation relationship between tumor volume, ventricle volume, and subcortical gray matter structures

	Tumor volume		Total lateral ventricle volume	
	rho	*P*	rho	*P*
Left thalamus	0.32	0.128	0.33	0.120
Left caudate	0.51	0.011	0.46	0.028
Left putamen	–0.47	0.023	0.02	0.919
Left pallidum	–0.71	0.000	–0.12	0.579
Left hippocampus	0.52	0.011	0.31	0.152
Left amygdala	–0.27	0.199	–0.48	0.021
Left accumbens area	–0.72	0.000	–0.42	0.048
Right thalamus	0.16	0.466	0.19	0.384
Right caudate	0.48	0.020	0.63	0.002
Right putamen	–0.59	0.003	–0.14	0.510
Right pallidum	–0.55	0.006	–0.02	0.919
Right hippocampus	0.40	0.052	0.33	0.120
Right amygdala	–0.27	0.207	–0.41	0.054
Right accumbens area	–0.48	0.018	–0.05	0.834

years that encompasses changes in executive function and working memory, visual-spatial impairments, difficulties in language production, and personality alterations.[12] It has been suggested that defects in the circuits between the cerebellum and prefrontal cortex caused by cerebellar masses could be one of the causes of this syndrome.[22] Indeed, a widespread gyral reduction in the frontal region was detected in our study. However, longitudinal and advanced imaging studies are needed to establish the correlation between these findings.

In patients with cerebellar tumors, failure of surface reconstruction has limited the investigation of surface-based morphometric changes in adult patients with intracranial tumors. A study by Zhang et al.[9] found decreased gyrification in bilateral medial orbitofrontal gyrus and lingual gyrus in the contralateral hemisphere of patients with frontal LGGs. Similarly, our study revealed widespread decreased gyrification in the cerebral cortex. While gyrification is associated with neurodevelopment, studies have also shown that axonal damage can disrupt gyrification.[23] Medulloblastomas are embryonal tumors that come with genetic mutations, particularly in the pediatric population. Therefore, the question of whether this global gyrification reduction is due to widespread axonal damage or folding abnormalities caused by accompanying genetic abnormalities should be supported by future genetic and longitudinal studies.

Recent studies have demonstrated that the basal ganglia and cerebellum form a connected network not only at the cortical level but also directly. Injection of rabies virus into the macaque putamen and globus pallidus externus significantly affected the cerebellum.[24] Our study demonstrated volume reduction in the putamen and pallidum in these patients, which may be associated with the involvement of this circuit. Recent functional MRI (fMRI) studies have identified a network involving the cerebellum, caudate nucleus, and prefrontal cortex, associated with executive functions, verbal fluency, and working memory. Abnormal activity in this network has been linked to diseases such as Alzheimer's disease.[25] Our study is the first to show a volume increase in the caudate nucleus and widespread cortical morphological changes in the frontal region in children with posterior fossa tumors, which may be associated with damage to the cerebello-ganglia-cortical network and subsequent impairment of executive functions. Future resting state fMRI studies in this population may support our findings.

The cerebellum is very important for functions such as balance and memory, as well as speech. It plays a crucial role in verbal fluency, grammar processing, and correcting language mistakes.[26] fMRI studies include the cerebellum in the language network along with the superior temporal lobe, pars triangularis, and precentral gyrus. These network clusters are predominantly in the left hemisphere, which is likely due to the language centers being primarily located in the left hemisphere in humans.[27] According to our findings, there is a reduction in volume asymmetrically in the left hemisphere in the pars triangularis and supramarginal gyrus, which are associated with the speech center. This may explain the areas showing volume reduction in the asymmetric left hemisphere and the asymmetry in the findings in these patients.

Recent studies have demonstrated a strong relationship between the cerebellum and the hippocampus. An experiment conducted in mice showed that optogenetic stimulation of the cerebellum resulted in changes in hippocampal functional connectivity and altered cellular dynamics.[28] Furthermore, recent studies have shown that the cerebellum is involved in various functions associated with memory. One such study in patients with hippocampal glioma revealed a compensatory volume increase in the contralateral hippocampus.[29] Similarly, the bilateral hippocampal volume increase in our study may be associated with this compensation. In opioid-dependent patients, there is decreased functional connectivity between the nucleus accumbens, amygdala, and cerebellum.[30] The decreased volume of the accumbens and amygdala in patients with cerebellar tumors may be due to the involvement of this circuit.

Our study has several limitations. First, this study is retrospective and was conducted at a single center. Our sample size was limited, and we did not categorize or assess tumors according to their subtypes and locations. However, it is worth noting that tumors situated in the vermis may influence distinct pathways compared with those located in the cerebellar hemispheres. Moreover, tumors in the posterior fossa were not staged. Nevertheless, the implications could differ between rapidly progressing tumors and those with slower growth rates. On the other hand, the changes we identified, irrespective of tumor grade or developmental stage, highlight the necessity and interest in further investigation into this matter. Second, even though there is no statistically significant difference between the groups in terms of the use of 1.5 Tesla and 3 Tesla devices, those used in the patient and control groups are not exactly balanced. A covariate has been used to counteract this, but it may have partially affected the results. There were no neurocognitive data available for the patients, and therefore the widespread changes in the brain could not be supported by neurocognitive data. Only structural MRI was used in this study, and the findings could not be supported by advanced techniques, such as diffusion tensor imaging or fMRI. Prospective studies may support our findings.

In conclusion, posterior fossa tumors lead to widespread morphological changes in cortical structures, with the most dominant pattern being hypogyrification, accompanied by a decreased surface area and volume reduction. Although cortical thickening predominantly increases, there are also areas where cortical thickness decreases. Subcortical gray matter structures, except for the hippocampus and caudate nucleus, showed volume reduction. These findings are highly correlated with the lateral ventricle volume. Other authors have nothing to disclose.

Conflict of interest disclosure

Meltem Necibe Ceyhan Bilgici, MD, is Section Editor in Diagnostic and Interventional Radiology. She had no involvement in the peer-review of this article and had no access to information regarding its peer-review.

References

1. Ward E, DeSantis C, Robbins A, Kohler B, Jemal A. Childhood and adolescent cancer statistics, 2014. *CA Cancer J Clin*. 2014;64(2):83-103. [CrossRef]
2. Muzumdar D, Ventureyra EC. Treatment of posterior fossa tumors in children. *Expert Rev Neurother*. 2010;10(4):525-546. [CrossRef]
3. Marchi V, Guzzetta A, Cioni G. Cerebral Plasticity and functional reorganization in children with congenital brain lesions. Neonatology, Springer International Publishing, 2017:1-10. [CrossRef]
4. Klein D, Mok K, Chen JK, Watkins KE. Age of language learning shapes brain structure: a cortical thickness study of bilingual and monolingual individuals. *Brain Lang*. 2014;131:20-24. [CrossRef]
5. Barrett KC, Ashley R, Strait DL, Kraus N. Art and science: how musical training shapes the brain. *Front Psychol*. 2013;4:713. [CrossRef]
6. Bates E, Reilly J, Wulfeck B, et al. Differential effects of unilateral lesions on language production in children and adults. *Brain Lang*. 2001;79(2):223-265. [CrossRef]
7. Lv K, Cao X, Wang R, et al. Contralesional macrostructural plasticity in patients with frontal low-grade glioma: a voxel-based morphometry study. *Neuroradiology*. 2023;65(2):297-305. [CrossRef]
8. Mills KL, Tamnes CK. Methods and considerations for longitudinal structural brain imaging analysis across development. *Dev Cogn Neurosci*. 2014;9:172-190. [CrossRef]
9. Zhang S, Sun H, Yang X, et al. An MRI study combining virtual brain grafting and surface-based morphometry analysis to investigate contralateral alterations in cortical morphology in patients with diffuse low-grade glioma. *J Magn Reson Imaging*. 2023;58(3):741-749. [CrossRef]
10. Buckner RL. The cerebellum and cognitive function: 25 years of insight from anatomy and neuroimaging. *Neuron*. 2013;80(3):807-815. [CrossRef]
11. Petersen KJ, Reid JA, Chakravorti S, et al. Structural and functional connectivity of the nondecussating dentato-rubro-thalamic tract. *Neuroimage*. 2018;176:364-371. [CrossRef]
12. Schmahmann JD, Sherman JC. The cerebellar cognitive affective syndrome. *Brain*. 1998;121(Pt 4):561-579. [CrossRef]
13. Zhang Y, Zou P, Mulhern RK, Butler RW, Laningham FH, Ogg RJ. Brain structural abnormalities in survivors of pediatric posterior fossa brain tumors: a voxel-based morphometry study using free-form deformation. *Neuroimage*. 2008;42(1):218-229. [CrossRef]
14. Fuentes D, Contreras J, Yu J, et al. Morphometry-based measurements of the structural response to whole-brain radiation. *Int J Comput Assist Radiol Surg*. 2015;10(4):393-401. [CrossRef]
15. Dietrich RB, Bradley WG, Zaragoza EJ 4th, et al. MR evaluation of early myelination patterns in normal and developmentally delayed infants. *AJR Am J Roentgenol*. 1988;150:889-896. [CrossRef]
16. Reid LB, Cunnington R, Boyd RN, Rose SE. Surface-based fMRI-driven diffusion tractography in the presence of significant brain pathology: a study linking structure and function in cerebral palsy. *PLoS One*. 2016;11(8):e0159540. [CrossRef]
17. Radwan AM, Emsell L, Blommaert J, et al. Virtual brain grafting: enabling whole brain parcellation in the presence of large lesions. *Neuroimage* 2021;229:117731. [CrossRef]
18. Iglesias JE, Billot B, Balbastre Y, et al. SynthSR: a public AI tool to turn heterogeneous clinical brain scans into high-resolution T1-weighted images for 3D morphometry. *Sci Adv*. 2023;9(5):1-14. [CrossRef]
19. Cuschieri S. The STROBE guidelines. *Saudi J Anaesth*. 2019;12(Suppl 1).31-34. [CrossRef]
20. Greve DN, Fischl B. False positive rates in surface-based anatomical analysis. *Neuroimage*. 2018;171:6-14. [CrossRef]
21. Ailion AS, Roberts SR, Crosson B, King TZ. Neuroimaging of the component white matter connections and structures within the cerebellar-frontal pathway in posterior fossa tumor survivors. *Neuroimage Clin*. 2019;23:101894. [CrossRef]
22. Hoche F, Guell X, Vangel MG, Sherman JC, Schmahmann JD. The cerebellar cognitive affective/Schmahmann syndrome scale. Brain. 2018;141(1):248-270. [CrossRef]
23. Li M, Hua K, Li S, et al. Cortical morphology of chronic users of codeine-containing cough syrups: association with sulcal depth, gyrification, and cortical thickness. *Eur Radiol*. 2019;29(11):5901-5909. [CrossRef]
24. Milardi D, Quartarone A, Bramanti A, et al. The Cortico-basal ganglia-cerebellar network: past, present and future perspectives. *Front Syst Neurosci*. 2019;13:61. [CrossRef]
25. Qi Z, An Y, Zhang M, Li HJ, Lu J. Altered cerebro-cerebellar limbic network in AD spectrum: a resting-state fMRI study. *Front Neural Circuits*. 2019;13.72. [CrossRef]
26. Leiner HC, Leiner AL, Dow RS. Cognitive and language functions of the human cerebellum. *Trends Neurosci*. 1993;16(11):444-447. [CrossRef]
27. Lipkin B, Tuckute G, Affourtit J, et al. Probabilistic atlas for the language network based on precision fMRI data from >800 individuals. *Sci Data*. 2022;9:529. [CrossRef]
28. Krook-Magnuson E, Szabo GG, Armstrong C, Oijala M, Soltesz I. Cerebellar directed optogenetic intervention inhibits spontaneous hippocampal seizures in a mouse model of temporal lobe epilepsy. *eNeuro*. 2014;1(1):ENEURO.0005-14.2014. [CrossRef]
29. Liu D, Chen J, Ge H, et al. Structural plasticity of the contralesional hippocampus and its subfields in patients with glioma. *Eur Radiol*. 2023;33(9):6107-6115. [CrossRef]
30. Moulton EA, Elman I, Becerra LR, Goldstein RZ, Borsook D. The cerebellum and addiction: insights gained from neuroimaging research. *Addict Biol*. 2014;19(3):317-331. [CrossRef]